Neuron
Report

Striatal Cholinergic Interneurons Drive GABA Release from Dopamine Terminals

Alexandra B. Nelson,[1,2] Nora Hammack,[1] Cindy F. Yang,[3] Nirao M. Shah,[3] Rebecca P. Seal,[4] and Anatol C. Kreitzer[1,2,5,*]
[1]The Gladstone Institutes, San Francisco, CA, 94158, USA
[2]Department of Neurology
[3]Department of Anatomy
University of California, San Francisco, San Francisco, CA 94158, USA
[4]Department of Neurobiology, University of Pittsburgh School of Medicine, Pittsburgh, PA 15213, USA
[5]Department of Physiology, University of California, San Francisco, San Francisco, CA 94158, USA
*Correspondence: akreitzer@gladstone.ucsf.edu
http://dx.doi.org/10.1016/j.neuron.2014.01.023

SUMMARY

Striatal cholinergic interneurons are implicated in motor control, associative plasticity, and reward-dependent learning. Synchronous activation of cholinergic interneurons triggers large inhibitory synaptic currents in dorsal striatal projection neurons, providing one potential substrate for control of striatal output, but the mechanism for these GABAergic currents is not fully understood. Using optogenetics and whole-cell recordings in brain slices, we find that a large component of these inhibitory responses derive from action-potential-independent disynaptic neurotransmission mediated by nicotinic receptors. Cholinergically driven IPSCs were not affected by ablation of striatal fast-spiking interneurons but were greatly reduced after acute treatment with vesicular monoamine transport inhibitors or selective destruction of dopamine terminals with 6-hydroxydopamine, indicating that GABA release originated from dopamine terminals. These results delineate a mechanism in which striatal cholinergic interneurons can co-opt dopamine terminals to drive GABA release and rapidly inhibit striatal output neurons.

INTRODUCTION

While they represent a sparse population of neurons within the striatum (1%–2%), cholinergic interneurons have been implicated in multiple striatal functions, including motor control, associative learning, and reward (Exley and Cragg, 2008; Shuen et al., 2008). Tonically active neurons (TANs), thought to be striatal cholinergic interneurons (Wilson et al., 1990), show precise patterns of firing during reward-based learning paradigms, suggesting a prominent role in plasticity (Cachope et al., 2012; Hanley and Bolam, 1997; Shen et al., 2005; Stuber et al., 2010). Although the precise mechanism by which cholinergic interneurons control striatal output has not yet been elucidated, recent studies provide interesting clues.

Activation of dorsal striatal cholinergic interneurons drives inhibitory responses in the principal cells of the striatum, medium spiny neurons (MSNs) and other cholinergic interneurons (English et al., 2012; Sullivan et al., 2008; Witten et al., 2010). Optogenetically evoked inhibitory postsynaptic currents (IPSCs) have two distinct components: a fast component (fIPSC) with a decay time constant of approximately 5 ms and a slower component (sIPSC) with a time constant of about 90 ms (English et al., 2012). Disynaptic inhibition via a rare striatal GABAergic interneuron subtype, neurogliaform cells, appears to explain a substantial portion of the sIPSC (English et al., 2012). However, the source of the fIPSC has not been identified.

In principle, the fIPSC may be monosynaptic or disynaptic. A disynaptic process would involve first a cholinergic synapse and then a GABAergic synapse. If disynaptic, two features of the fIPSC are as yet unclear: (1) whether cholinergic control of GABA release is mediated by axon-to-dendrite versus axon-to-axon-terminal neurotransmission, and (2) what cell type releases GABA. Two cell types are good candidates by virtue of being activated by nicotinic receptors and their ability to drive large, fast inhibitory responses in MSNs: fast-spiking interneurons (FSIs) (Koós and Tepper, 2002) and nigrostriatal dopaminergic neurons (Cachope et al., 2012; Exley and Cragg, 2008; Threlfell et al., 2012; Zhou et al., 2001). Recent experiments have also demonstrated that dopaminergic neurons can release both dopamine and GABA, both of which depend on the vesicular monoamine transporter (VMAT) (Tritsch et al., 2012).

Here, we test the potential roles of striatal FSIs and dopamine terminals in mediating cholinergically triggered disynaptic IPSCs in MSNs. Using a combination of methods, we demonstrate that the fast portion of the IPSC is mediated by cholinergic activation of GABA release from striatal dopaminergic terminals, which is action potential independent. These findings suggest that cholinergic interneurons are able to rapidly regulate striatal output through GABAergic inhibition, while simultaneously exerting neuromodulatory control via dopamine and acetylcholine signaling.

RESULTS

We used an optogenetic approach to explore how cholinergic interneuron activity influences striatal output neurons. Injection

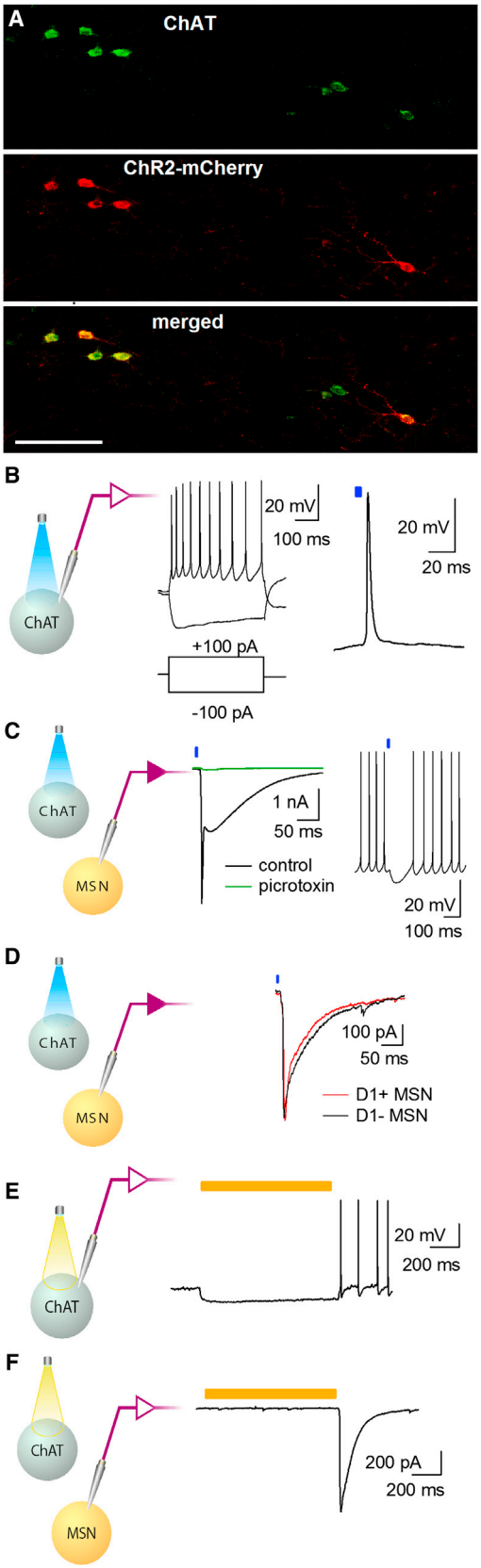

Figure 1. Optogenetic Activation of Striatal Cholinergic Interneurons Elicits Inhibitory Synaptic Responses

(A–D) Dorsal striatal slices from ChAT-Cre mice injected with AAV2/1-DIO-ChR2-mCherry. (A) Immunohistochemistry for ChAT (top), mCherry (middle), and merged (bottom), showing mCherry-positive neurons were positive for ChAT. Scale bar, 100 μm. (B) Left: recording configuration. Current-clamp recording from an mCherry-positive, putative cholinergic interneuron. Membrane potential responses to injection of ±100 pA (middle) or a single 5 ms light pulse (470 nM, blue bar; right). (C) Left: recording configuration. Middle: voltage-clamp recording from a medium spiny neuron (MSN). Blue light pulses evoked a large inward current with two phases before (black) and after (green) application of picrotoxin (50 μM). Right: current-clamp recording from an MSN depolarized to fire action potentials. A blue light pulse caused a brief pause in the firing of the MSN. (D) Left: recording configuration. Right: synaptic currents from a D1-Tomato-positive MSN (red trace) and a nearby D1-Tomato-negative MSN (black trace) in response to blue light pulses. (E and F) Recordings made in ChAT-Cre mice injected with AAV5-DIO-eNpHR3.0-YFP. (E) Left: recording configuration. Right: current-clamp recording from a YFP-positive, putative cholinergic interneuron, showing hyperpolarization followed by rebound firing in response to a 1,000 ms light pulse (554 nm, yellow bar). (F) Left: recording configuration. Right: a large IPSC in an MSN at the offset of the light pulse.

of a Cre-dependent virus (AAV2/1-DIO-ChR2-mCherry) encoding channelrhodopsin-2 (ChR2) in the dorsal striatum of choline acetyltransferase (ChAT)-Cre mice produced selective ChR2 expression in striatal cholinergic interneurons (Figure 1A).

To physiologically confirm ChR2 expression in cholinergic interneurons, we performed whole-cell current-clamp recordings of mCherry-positive neurons. These neurons showed typical intrinsic properties, including spontaneous action potential firing, pronounced action potential afterhyperpolarization, and a characteristic voltage sag with hyperpolarizing current (Kawaguchi, 1993) (Figure 1B). Brief (5 ms) blue light pulses triggered action potentials in mCherry-positive putative cholinergic neurons (Figure 1B).

To isolate inhibitory synaptic currents triggered by activation of cholinergic neurons, we performed whole-cell voltage-clamp recordings of medium spiny neurons in the presence of glutamate receptor antagonists NBQX and D-APV. Using a high-chloride internal solution to promote detection of GABAergic currents, blue light pulses elicited IPSCs measuring 1,830 ± 290 pA (n = 37). This light-evoked IPSC was characterized by distinct phases of decay, as has been described previously (English et al., 2012): the fIPSC had a decay time constant of 5.2 ± 1.0 ms, while an sIPSC had a decay time constant of 90 ± 7 ms (Figure 1C). Both IPSC phases were blocked by the $GABA_A$ antagonist picrotoxin (50 μM; 98% ± 0.4% block; n = 6; p = 0.009; Figure 1C), which was shown previously with bicuculline (English et al., 2012), confirming that the IPSC is GABAergic. Delivery of two blue light pulses at short intervals produced IPSCs with marked paired-pulse depression; full recovery of the IPSC occurred between 30 and 60 s (Figure S1 available online). Single blue light pulses could block action potentials in MSNs under physiological conditions (see example, Figure 1C), demonstrating the potential functional relevance of these inhibitory responses. To determine whether light-evoked IPSCs differed between direct- and indirect-pathway medium spiny neurons, a subset of experiments were performed in ChAT-Cre:Drd1a-Tomato mice, which express the fluorescent reporter tdTomato in dopamine D1 receptor-containing neurons

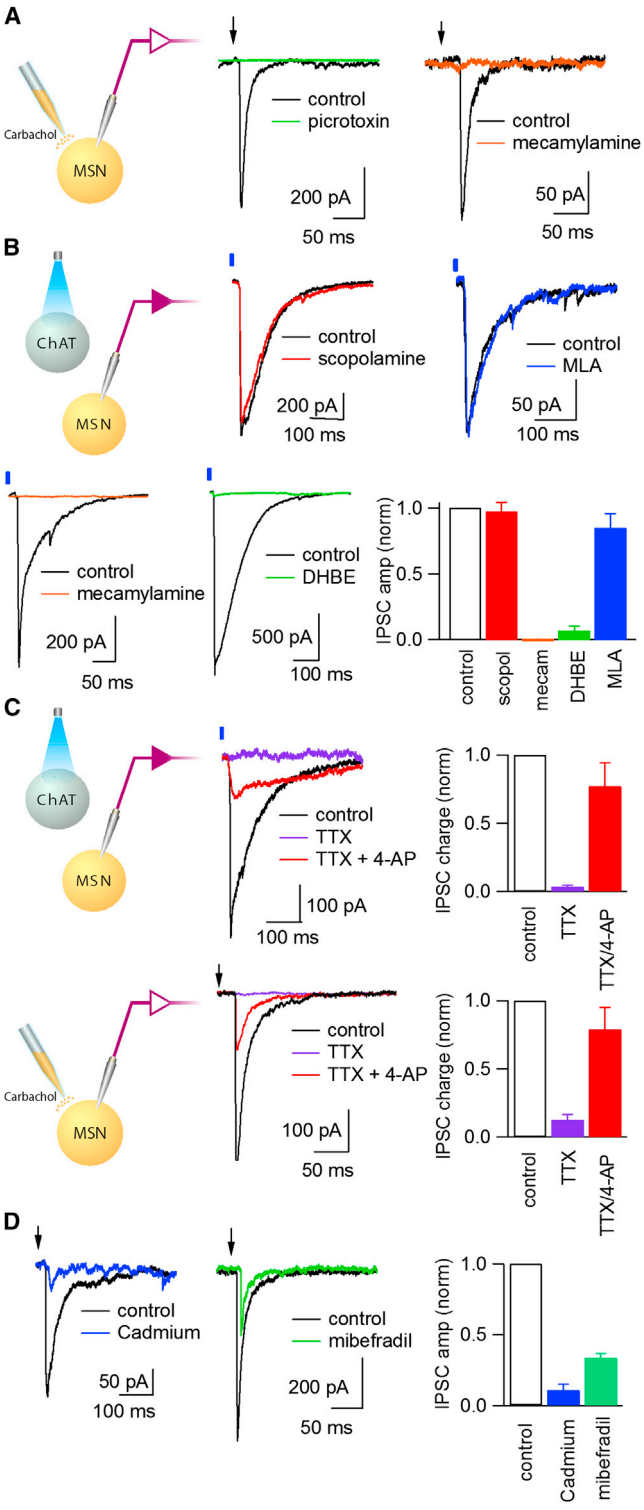

Figure 2. Disynaptic Inhibitory Synaptic Responses Are Action Potential Independent

(A) Voltage-clamp recording from an MSN, showing the inward current triggered by carbachol (10 mM), locally pressure ejected from a pipet positioned nearby (schematic at left). The carbachol-evoked current is shown before (black) and after (green) bath application of picrotoxin (50 μM; middle) and before (black) and after (orange) bath application of the nicotinic antagonist mecamylamine (5 μM; right). (B) Representative light-evoked inhibitory synaptic responses (schematic at left) before (black) and after application of the muscarinic antagonist scopolamine (10 μM, red), the nicotinic antagonists mecamylamine (5 μM, orange) and dihydrobetaerythroidine (DHβE; 10 μM, green), and the a7 nicotinic antagonist methyllycaconitine (MLA; 10 nM, blue). Right: normalized IPSC amplitude. (C) Top: light-activated IPSCs in MSNs (schematic at left). The disynaptic IPSC (black) was abolished by bath application of tetrodotoxin (TTX; 1 μM, purple) then partly restored by TTX + 4-aminopyridine (4-AP; 100 μM, red). Right: normalized net IPSC charge. Bottom: carbachol-evoked IPSCs in MSNs (schematic at left) at baseline (black) and after TTX (purple) and TTX + 4-AP (red). Right: normalized net IPSC charge. (D) Carbachol-evoked IPSCs in MSNs at baseline (black trace) and after application of cadmium chloride (100 μM; left, blue trace) or mibefradil (100 μM; middle, green trace). Right: normalized IPSC amplitude. All bars represent mean ± SEM.

(Shuen et al., 2008). Optogenetically evoked IPSCs were comparable in interleaved D1-Tomato-positive and -negative MSNs (Figure 1D), measuring 990 ± 210 pA (n = 14) and 920 ± 110 pA (n = 12, p = 0.6), respectively. To determine whether rebound firing by cholinergic interneurons could also drive IPSCs, the inhibitory opsin halorhodopsin (eNpHR3.0) was expressed in cholinergic interneurons. In ChAT-Cre mice injected with AAV5-DIO-eNpHR3.0-YFP, yellow light caused hyperpolarization of the membrane potential in cholinergic interneurons and, at the offset of such pulses, rebound spiking (Figure 1E). Voltage-clamp recordings of MSNs showed large IPSCs at the offset of yellow light pulses (Figure 1E), which were similar in amplitude (1,130 ± 230 pA; n = 5) and kinetics (tau decay times for fast and slow components 6.2 ± 1.5 and 127.6 ± 28.2 ms, respectively) to IPSCs elicited with ChR2 activation. These findings suggest that cholinergic interneuron activity, triggered by direct depolarization or rebound following hyperpolarization, can lead to large IPSCs in MSNs.

Light-evoked IPSCs could, in principle, be derived from monosynaptic GABA release by cholinergic interneurons themselves, as has been shown in the retina (Lee et al., 2010), or through a disynaptic mechanism (Figure S2). A disynaptic mechanism should depend on transmitter release from cholinergic interneurons onto a second class of GABA-containing neurons. Indeed, the fast portion of the IPSC was reconstituted by local application of the cholinergic agonist carbachol (10 mM) near the recorded MSN. Carbachol produced large-amplitude IPSCs (850 ± 160 pA, n = 11), which were blocked by picrotoxin (50 μM; Figure 2A). This carbachol-triggered IPSC had a tau decay of 7.2 ± 1.1 ms (n = 11) comparable to the fast component of the light-evoked IPSC, suggesting that local application could selectively recruit GABA release responsible for the fIPSC. Carbachol-triggered IPSCs were also blocked by the nicotinic antagonist mecamylamine (5 μM; Figure 2A), indicating that they are mediated by nicotinic acetylcholine receptors. Dependence of light-evoked responses on acetylcholine release was confirmed using cholinergic receptor antagonists. IPSC amplitude was not significantly reduced by the muscarinic antagonist scopolamine (10 μM; 3% ± 7% block; n = 5; p = 0.39) or the α7 nicotinic receptor antagonist methyllycaconitine (MLA, 10 nM; 15% ± 11% block; n = 7; p = 0.14) but was potently inhibited by the nicotinic antagonists mecamylamine (5 μM; 97% ± 2%

block; n = 5; p = 0.038) and dihydrobetaerythroidine (DHβE, 10 μM; 93% ± 3% block; n = 5; p = 0.034; Figure 2B). These experiments demonstrated that the IPSC depends on non-α7-containing nicotinic acetylcholine receptors and suggested a disynaptic mechanism.

Disynaptic IPSCs could derive from cholinergic stimulation of an action potential in a second neuron, resulting in action-potential-dependent release of GABA onto MSNs. Alternatively, acetylcholine could activate nicotinic receptors at sites of GABA release, eliciting IPSCs in MSNs without a requirement for action potentials (see Figure S2). To investigate this latter possibility, we activated cholinergic interneurons and recorded IPSCs in MSNs while applying the sodium channel antagonist tetrodotoxin (TTX, 1 μM), which would be expected to block action potentials in both the cholinergic interneuron and putative GABAergic neurons. TTX application resulted in a complete block of the disynaptic IPSC (Figure 2C). However, application of TTX together with the potassium channel antagonist 4-aminopyridine (4-AP, 100 μM), which enables ChR2-mediated release of neurotransmitter without action potentials (Petreanu et al., 2012), partially restored the IPSC (Figure 2C). The average amplitude of IPSCs after addition of TTX and 4-AP was 43% ± 11% (n = 14) of the control IPSC, and the area under the IPSC (net charge) after addition of TTX and 4-AP was 77% ± 17% of the control IPSC (n = 14; Figure 2C). Using a similar method, the net charge of the carbachol-triggered IPSC in the presence of TTX and 4-AP was 79% ± 16% of control (n = 6; Figure 2C). These results support the hypothesis that a substantial portion of the IPSC triggered by cholinergic interneuron stimulation is through an action-potential-independent mechanism.

Though activation of nicotinic receptors led to GABA release, it was unclear whether synaptic vesicle release was triggered directly by calcium influx through nicotinic receptors or through recruitment of additional calcium sources, such as voltage-gated calcium channels or internal calcium stores. As optogenetically evoked IPSCs were blocked by DHβE but not by MLA, the nicotinic receptors involved are a non-α7-containing subtype, with lower calcium permeability (Rice and Cragg, 2004), and are thus less likely to participate directly in vesicle fusion. Suspecting voltage-gated calcium channels might provide the necessary calcium, we elicited IPSCs with pressure-ejected carbachol and applied cadmium chloride, a nonselective blocker of voltage-gated calcium channels that does not block α4-containing nicotinic receptors (Karadsheh et al., 2004). Cadmium markedly reduced IPSC amplitude (n = 5; p = 0.01; Figure 2D), suggesting voltage-gated calcium channels are required for nicotinic activation of GABA release. In the hippocampus, nicotinic depolarization of axon terminals triggers GABA release through T-type calcium channels (Tang et al., 2011), so we proceeded to test the role of these channels in light-evoked disynaptic inhibition. The specific T-type calcium channel blocker mibefradil (5 μM) reduced the light-evoked IPSC by 41% ± 6% (n = 8, p = 0.02; data not shown) and the carbachol-evoked IPSC by 67% ± 3% (n = 4; Figure 2D). Together, these results suggest that presynaptic nicotinic receptor activation leads to the recruitment of voltage-gated calcium channels, including T-type channels, to cause sufficient calcium influx for release of GABA onto MSNs.

While these findings suggest that the fIPSC triggered by activation of cholinergic interneurons is likely to be disynaptic and action potential independent, they do not indicate which neurons release GABA. FSIs drive large inhibitory synaptic responses in MSNs, making them a candidate source of GABA for the fast disynaptic ISPC (Gittis et al., 2010; Koós and Tepper, 1999). To determine whether FSIs are required for disynaptic inhibition, we selectively ablated a majority of the parvalbumin (PV)-positive FSIs by injecting the striatum of PV-Cre mice (Figure 3A) with a Cre-dependent virus encoding pro-caspase-3 and an enzyme that cleaves pro-caspase-3 into the active, proapoptotic signal caspase-3 (Yang et al., 2013). PV-positive cells were greatly diminished in the AAV-FLEX-taCasp3-TEVp-injected striatum as compared to the contralateral control striatum (3 ± 1 versus 56 ± 6 PV-positive dorsal striatal neurons per section; n = 7 mice; Figures 3B and 3C). As a positive control that this manipulation could eliminate monosynaptic inhibition from FSI onto MSN, we injected PV-Cre mice with bilateral AAV1-DIO-ChR2-YFP and unilateral AAV1-FLEX-taCasp3-TEVp. Slices contralateral to AAV1-FLEX-taCasp3-TEVp injection showed expression of ChR2-YFP in PV-positive putative FSI (Figure S3B), while in ipsilateral slices very few PV-positive neurons were detected (Figures 3B, 3C, and S3A); most of these remaining neurons expressed ChR2-YFP. Presumed monosynaptic FSI-mediated IPSCs were large in control slices (5,880 ± 530 pA; n = 7) but negligible in caspase-treated slices (30 ± 8 pA; n = 13, n = 3 mice; p = 0.0001; Figure 3C), demonstrating that near-complete elimination of PV neurons resulted in near-complete loss of the FSI-mediated IPSC in MSNs. To determine whether elimination of PV-positive neurons and their input onto MSNs would likewise reduce the disynaptic IPSC derived from activation of cholinergic interneurons, we injected AAV1-FLEX-taCasp3-TEVp unilaterally in ChAT-ChR2::PV-Cre mice. In these mice, ChR2 is expressed constitutively in cholinergic interneurons (Zhao et al., 2011). Interestingly, ablation of PV-positive neurons (Figures 3B and 3D) did not significantly alter light-evoked disynaptic IPSCs (1,110 ± 370 pA; n = 18 neurons/n = 4 mice in the injected hemisphere versus 960 ± 340 pA; n = 13 neurons/n = 4 mice in the untreated hemisphere; p = 0.79; Figure 3D). These results demonstrate that FSIs are not required for disynaptic IPSCs and suggest that the majority of the fIPSC is derived from an alternate source of GABA.

Given that (1) optogenetic activation of cholinergic interneurons can drive terminal dopamine release in the striatum (Cachope et al., 2012; Threlfell et al., 2012), and (2) anatomical studies (Campbell et al., 1991; González-Hernández et al., 2001) and a recent physiological study (Tritsch et al., 2012) suggest striatal dopaminergic axon terminals may release GABA, we hypothesized that the fIPSC was derived from cholinergic activation of dopaminergic axon terminals, resulting in GABA release. To test this hypothesis, we compared disynaptic IPSCs in slices from animals treated unilaterally with saline (control) or the dopaminergic neurotoxin 6-hydroxydopamine (6-OHDA). Degeneration of dopaminergic axons ipsilateral to the injection was confirmed by post hoc tyrosine hydroxylase staining (Figure 4A). 6-OHDA treatment resulted in markedly reduced light-evoked IPSCs (170 ± 40 pA, n = 14 neurons/n = 4 mice) as compared to saline treatment (Figures 4B and 4C; 1,610 ± 410 pA, n = 10

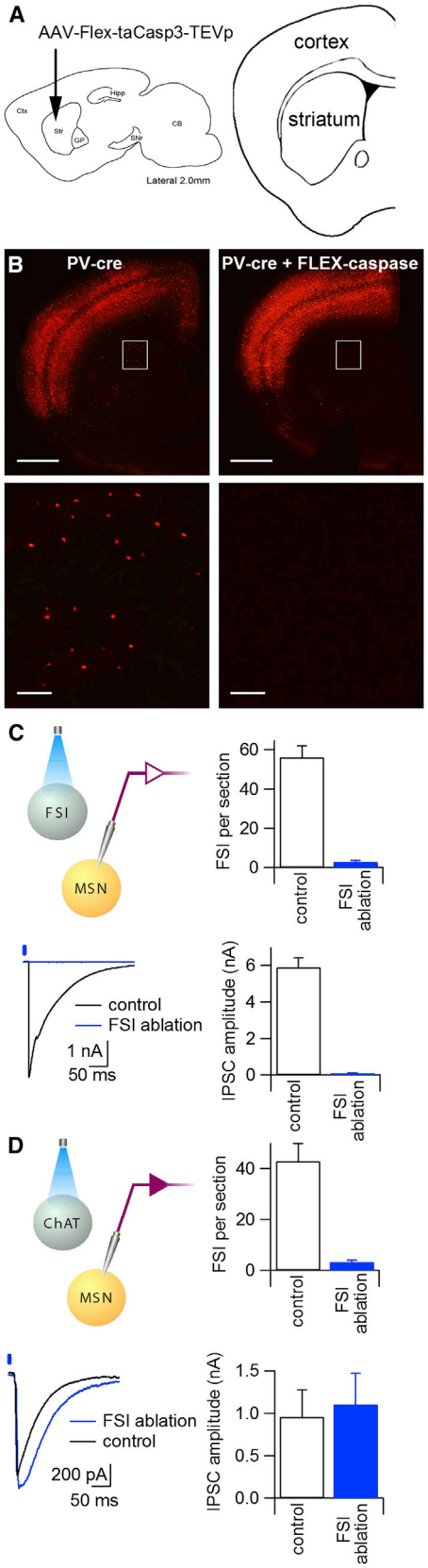

Figure 3. Ablation of Parvalbumin-Positive Fast-Spiking Interneurons Does Not Alter the Disynaptic IPSC

The dorsolateral striatum of PV-Cre mice was injected with AAV1-FLEX-taCasp3-TEVp to ablate parvalbumin (PV)-positive neurons. (A) Top: diagrams of the brain in sagittal view (left), showing the area of viral injection, and coronal view (right), showing the structures in histological sections below. (B) Coronal sections immunostained for PV (red). Top: control (uninjected) hemisphere (left) and hemisphere injected with AAV1-FLEX-taCasp3-TEVp (right). Scale bar, 1 mm. Inset: area of dorsal striatum where physiological recordings were made. Bottom: control (uninjected, left) and FSI-ablation (injected, right) sections, showing striatal PV-positive neurons. Scale bar, 150 μm. (C) Recordings made from PV-Cre mice injected with bilateral AAV1-DIO-ChR2-YFP and unilateral AAV1-FLEX-taCasp3-TEVp. Top left: recording configuration. Top right: average number of PV-positive neurons per hemisection of the dorsal striatum in control (ChR2 only) and FSI ablation (ChR2 + caspase) conditions. Bottom left: representative light-activated (presumed monosynaptic) currents elicited in MSNs in the control (black) and FSI ablation (blue) conditions. Bottom right: average IPSC amplitude in control versus FSI ablation slices. (D) Recordings made from PV-Cre:ChAT-ChR2 mice injected with unilateral AAV1-FLEX-taCasp3-TEVp. Top left: recording configuration. Top right: average number of PV-positive neurons per hemisection of the dorsal striatum in control and FSI ablation conditions. Bottom left: representative light-activated (presumed disynaptic) currents in MSNs in control (black) and FSI ablation (blue) conditions. IPSCs recorded at −70 mV in the presence of NBQX and APV. Bottom right: average IPSC amplitude in control versus FSI ablation slices. All bars represent mean ± SEM.

neurons/n = 3 mice, p = 0.0006). This result suggests that the fIPSC triggered by activation of cholinergic interneurons depends on the integrity of nigrostriatal dopamine neurons. To further investigate whether depletion of neurotransmitter from dopamine terminals alters IPSC amplitude, we compared disynaptic IPSCs in slices from mice treated with the VMAT inhibitor reserpine and interleaved control mice. Although a provocative finding, a prior study showed that inhibition of VMAT prevented dopamine and GABA release from striatal dopamine terminals (Tritsch et al., 2012). We found markedly reduced IPSC amplitudes in reserpine-treated mice (240 ± 40 pA, n = 19; n = 3 mice) compared to interleaved control mice (Figures 4B and 4C; 1,760 ± 90 pA, n = 14; n = 5 mice; p = 0.0001), indicating that IPSCs depend on VMAT. Surprisingly, 6-OHDA and reserpine treatment resulted in reductions of both fast and slow IPSC components: neuropeptide Y-expressing neurogliaform (NPY-NGF) neurons contribute prominently to the sIPSC (English et al., 2012). Suspecting that the chronicity of 6-OHDA and reserpine treatment might lead to striatal microcircuit reorganization and downregulation of the NPY-NGF-mediated sIPSC, we next used the more rapid-acting VMAT inhibitors Ro4-1284 and tetrabenazine (TBZ). These two agents were administered either in vivo immediately before slicing (Ro4-1284) or ex vivo to slices (TBZ). Acute Ro4-1284 treatment also reduced the amplitude of disynaptic IPSCs (670 ± 170 pA; n = 13 neurons/n = 2 mice) as compared to Ro4-1284 treatment followed by artificial cerebrospinal fluid (ACSF) wash for at least 1 hr (Figures 4B and 4C; 1,840 ± 360 pA; n = 12 neurons/n = 2 mice; p = 0.006) but left a substantial residual sIPSC. TBZ treatment decreased IPSC amplitude (740 ± 130 pA; n = 7 neurons/n = 3 mice) compared to interleaved controls (Figures 4B and 4C; 2,570 ± 770 pA; n = 9 neurons/n = 3 mice; p = 0.04), also leaving a residual sIPSC (decay tau 152 ± 26 ms). To verify that the decreased amplitude of IPSCs was not due to loss of dopamine-mediated

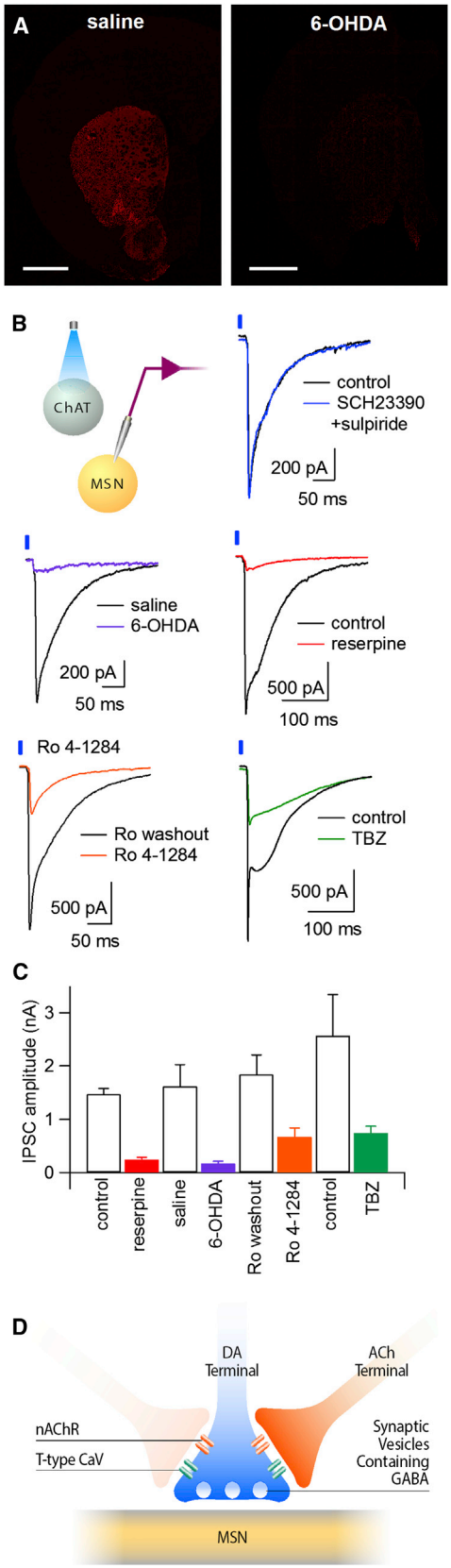

Figure 4. Disynaptic Inhibitory Responses Require Dopaminergic Neurons

(A) Coronal sections containing the striatum immunostained for tyrosine hydroxylase (red). Left: striatum of mouse injected with saline. Right: striatum of mouse injected with 6-OHDA. Scale bar, 1 mm. (B) Recording configuration. Representative light-evoked currents in MSNs from ChAT-Cre animals injected with striatal AAV2/1-DIO-ChR2-mCherry. IPSCs are shown at baseline (black) versus after 10 min application of SCH23390 (1 μM) and sulpiride (10 μM, blue); in slices from saline-injected (black) versus 6-OHDA-injected (purple) mice; interleaved control (black) versus reserpine-injected (red) mice; Ro4-1284-incubated (orange) versus Ro4-1284 washout (black) slices from the same Ro4-1284-injected mice; and tetrabenazine-treated (green) versus interleaved control (black) mice. (C) Summary of light-evoked IPSCs. (D) Schematic diagram of proposed microcircuit involving striatal cholinergic interneurons (red), nigrostriatal dopamine terminals (blue), and medium spiny neuron dendrites (yellow). All bars represent mean ± SEM.

neuromodulation of the IPSC itself, we applied a cocktail of D1 and D2 dopamine receptor antagonists (SCH23390, 1 μM; sulpiride, 10 μM) to control slices. Dopamine antagonists did not significantly alter IPSC amplitude (Figure 4B; 94% ± 8% of control, n = 6; p = 0.54). Together, these findings strongly suggest that dopaminergic terminals provide a major source of the GABA underlying fast disynaptic IPSCs seen in MSNs after stimulation of cholinergic interneurons, as schematized in Figure 4D.

DISCUSSION

We have demonstrated that optogenetic activation of striatal cholinergic neurons triggers a disynaptic inhibitory synaptic response in MSNs, mediated in large part by nicotinic activation of GABA release from dopamine terminals. Surprisingly, parvalbumin-positive FSIs, a major source of GABAergic inputs to MSNs, are not required. As this phenomenon is TTX insensitive, and axons are the only portion of dopamine neurons present in our preparation, acetylcholine appears to trigger striatal GABA release via an action-potential-independent axoaxonic mechanism. These findings link prior studies showing (1) inhibitory responses in MSNs driven by optogenetic activation of striatal cholinergic interneurons, (2) inhibitory responses in MSNs driven by optogenetic activation of striatal dopamine terminals, and (3) dopamine release driven by optogenetic activation of striatal cholinergic interneurons and provide a mechanism by which striatal cholinergic interneurons may potently influence striatal output by dual control of dopamine and GABA release.

One potential caveat of our study and others using BAC transgenic animals for optical control of cholinergic neurons is that ChAT-ChR2 mice have recently been found to have elevated ACh release and cognitive deficits due to overexpression of vesicular ACh transporters (Kolisnyk et al., 2013). Increased ACh release may enhance the amplitude of ACh-dependent responses but is unlikely to alter the overall mechanisms that we have outlined.

The finding that fast GABAergic currents in MSNs derive from dopamine terminals is intriguing. Though dopamine axon terminals do not always form traditional tight axodendritic synapses onto MSNs (Descarries et al., 1996), they do form a relatively uniform and dense lattice of inputs in the dorsal striatum (Hanley and Bolam, 1997), and dopamine may influence postsynaptic targets over a broad area encompassing tens of thousands of

synapses (Rice and Cragg, 2008). Terminal GABA release may also operate via volume transmission or, alternatively, the IPSCs we observe may arise from GABA release at dopamine terminals that are located proximal to GABAergic synapses.

Optogenetics provide a tool for synchronous selective activation of striatal cholinergic interneurons, but prior anatomical and physiological studies have outlined much of the signaling substrate. Nicotinic acetylcholine receptors reside on dopaminergic axon terminals (Jones et al., 2001; Threlfell et al., 2010), providing the anatomical means for acetylcholine to drive the release of dopamine (and GABA) from axon terminals in the striatum. In addition, the regulation of dopamine release by nicotinic receptors has been demonstrated directly (Rice and Cragg, 2004; Zhang and Sulzer, 2004; Zhou et al., 2001). These studies have shown that while phasic cholinergic stimulation can cause dopamine release, more prolonged stimulation results in nicotinic receptor desensitization and reduced release, which may be responsible for many of the behavioral pharmacology results obtained with nicotinic agents in vivo. By allowing precisely timed, synchronous release of acetylcholine and subsequent stimulation of nicotinic receptors, optogenetic strategies have facilitated detecting phasic responses in the striatum, which appear to be opposite in polarity to those seen with more tonic manipulations of acetylcholine.

Despite evidence that cholinergic signaling is critical for striatal behaviors, how cholinergic interneurons alter striatal output is unclear. Spontaneously firing cholinergic interneurons receive strong excitatory thalamic input, which carries cue-related information, and inhibitory inputs from midbrain GABAergic neurons (Brown et al., 2012). In many in vivo studies, cholinergic neurons display a burst-pause-burst pattern of firing during relevant cues in the context of learned tasks. Cholinergic neurons send their projections widely throughout the striatum, influencing most striatal neurons through muscarinic or nicotinic receptors. Nicotinic receptor activation may have distinct phasic and tonic effects on MSNs due to the prominent desensitization of many nicotinic subtypes. The stereotyped burst-pause-burst firing pattern of cholinergic neurons could allow for (1) a window of relief from desensitization and (2) a more concerted modulation of MSN firing by release of fast-acting GABA and longer-acting dopamine during the burst. Afterward, spontaneous firing of cholinergic interneurons could again result in nicotinic desensitization and reduced dopamine and GABA release. These same processes may also influence the cholinergic interneurons themselves, given the proximity of dopamine terminals and cholinergic interneurons. While the significance of each of these mechanisms to the function of striatal cholinergic interneurons in vivo is not yet known, the ability of these neurons to recruit both dopamine and GABA release to modulate striatal output is likely to significantly contribute to their influence of basal ganglia function.

EXPERIMENTAL PROCEDURES

Detailed methods are in Supplemental Experimental Procedures.

Animals

Hemizygous ChAT-Cre mice (line GM60, GENSAT) were bred against either wild-type C57Bl/6 mice (The Jackson Laboratory) or Drd1a-tdTomato mice (Nicole Calakos, Duke University) to yield ChAT-Cre or ChAT-Cre:Drd1a-tdTomato mice. Hemizygous ChAT-ChR2 mice (The Jackson Laboratory) were crossed to Parvalbumin-2A-Cre mice (The Jackson Laboratory) to yield ChAT-ChR2:PV-Cre mice. Mice of either sex were used.

Surgery

Virus was stereotactically injected in the dorsal striatum of mice through a small hole in the skull. Mice returned to their home cages for 2–4 weeks prior to histology or physiology. Some mice were later reanesthetized and injected with either the toxin 6-hydroxydopamine or normal saline in the medial forebrain bundle.

Physiology

Mice were deeply anesthetized prior to removing the brain and preparing 300 μm coronal slices. Slices were stored in carbogenated ACSF at room temperature (RT) and then transferred to a recording chamber superfused with carbogenated ACSF at 31°C–33°C. Neurons were patched in the dorsal striatum in whole-cell mode, and ChR2 or eNpHR3.0 was activated with light pulses delivered through the microscope objective. With the exception of carbachol, which was pressure ejected from a glass pipet, drugs were administered in the circulating ACSF.

Histology

A subset of mice was deeply anesthetized, perfused, and fixed. Brains were removed, cryoprotected, frozen, and cut into 30 μm coronal sections. Primary antibody (Millipore AB144P Anti-ChAT 1:500, SWANT Anti-parvalbumin 1:1,000, or Pel-Freez P40101 Anti-Tyrosine Hydroxylase 1:1,000) was added in 5% NDS, 1% Triton in PBS and incubated overnight at 4°C. After washing, slices were incubated with Alexa Fluor 649-conjugated donkey anti-goat or donkey anti-rabbit secondary antibody (Invitrogen) for 2 hr at RT.

Statistics

All data are presented as the mean ± SEM. Comparisons were made using the Student's t test.

SUPPLEMENTAL INFORMATION

Supplemental Information includes Supplemental Experimental Procedures and three figures and can be found with this article online at http://dx.doi.org/10.1016/j.neuron.2014.01.023.

ACKNOWLEDGMENTS

Funded by the A.P. Giannini Research fellowship (A.B.N.), NINDS K08 NS081001 (A.B.N.), NINDS R01 NS064984 and R01 NS078435 (A.C.K.), NINDS RO1 NS082650 (R.P.S.), and NINDS R01 NS049488 and R01 NS083872 (N.M.S.). We thank Dan Gray and Jim Wells for their help in generating the FLEX-taCasp3-TEVp construct and Diane Nathaniel and Delanie Schulte for technical assistance.

Accepted: January 13, 2014
Published: March 6, 2014

REFERENCES

Brown, M.T., Tan, K.R., O'Connor, E.C., Nikonenko, I., Muller, D., and Lüscher, C. (2012). Ventral tegmental area GABA projections pause accumbal cholinergic interneurons to enhance associative learning. Nature *492*, 452–456.

Cachope, R., Mateo, Y., Mathur, B.N., Irving, J., Wang, H.L., Morales, M., Lovinger, D.M., and Cheer, J.F. (2012). Selective activation of cholinergic interneurons enhances accumbal phasic dopamine release: setting the tone for reward processing. Cell Rep. *2*, 33–41.

Campbell, K.J., Takada, M., and Hattori, T. (1991). Co-localization of tyrosine hydroxylase and glutamate decarboxylase in a subpopulation of single nigrotectal projection neurons. Brain Res. *558*, 239–244.

Descarries, L., Watkins, K.C., Garcia, S., Bosler, O., and Doucet, G. (1996). Dual character, asynaptic and synaptic, of the dopamine innervation in adult

rat neostriatum: a quantitative autoradiographic and immunocytochemical analysis. J. Comp. Neurol. *375*, 167–186.

English, D.F., Ibanez-Sandoval, O., Stark, E., Tecuapetla, F., Buzsáki, G., Deisseroth, K., Tepper, J.M., and Koos, T. (2012). GABAergic circuits mediate the reinforcement-related signals of striatal cholinergic interneurons. Nat. Neurosci. *15*, 123–130.

Exley, R., and Cragg, S.J. (2008). Presynaptic nicotinic receptors: a dynamic and diverse cholinergic filter of striatal dopamine neurotransmission. Br. J. Pharmacol. *153* (*Suppl 1*), S283–S297.

Gittis, A.H., Nelson, A.B., Thwin, M.T., Palop, J.J., and Kreitzer, A.C. (2010). Distinct roles of GABAergic interneurons in the regulation of striatal output pathways. J. Neurosci. *30*, 2223–2234.

González-Hernández, T., Barroso-Chinea, P., Acevedo, A., Salido, E., and Rodríguez, M. (2001). Colocalization of tyrosine hydroxylase and GAD65 mRNA in mesostriatal neurons. Eur. J. Neurosci. *13*, 57–67.

Hanley, J.J., and Bolam, J.P. (1997). Synaptology of the nigrostriatal projection in relation to the compartmental organization of the neostriatum in the rat. Neuroscience *81*, 353–370.

Jones, I.W., Bolam, J.P., and Wonnacott, S. (2001). Presynaptic localisation of the nicotinic acetylcholine receptor beta2 subunit immunoreactivity in rat nigrostriatal dopaminergic neurones. J. Comp. Neurol. *439*, 235–247.

Karadsheh, M.S., Shah, M.S., Tang, X., Macdonald, R.L., and Stitzel, J.A. (2004). Functional characterization of mouse alpha4beta2 nicotinic acetylcholine receptors stably expressed in HEK293T cells. J. Neurochem. *91*, 1138–1150.

Kawaguchi, Y. (1993). Physiological, morphological, and histochemical characterization of three classes of interneurons in rat neostriatum. J. Neurosci. *13*, 4908–4923.

Kolisnyk, B., Guzman, M.S., Raulic, S., Fan, J., Magalhães, A.C., Feng, G., Gros, R., Prado, V.F., and Prado, M.A. (2013). ChAT-ChR2-EYFP mice have enhanced motor endurance but show deficits in attention and several additional cognitive domains. J. Neurosci. *33*, 10427–10438.

Koós, T., and Tepper, J.M. (1999). Inhibitory control of neostriatal projection neurons by GABAergic interneurons. Nat. Neurosci. *2*, 467–472.

Koós, T., and Tepper, J.M. (2002). Dual cholinergic control of fast-spiking interneurons in the neostriatum. J. Neurosci. *22*, 529–535.

Lee, S., Kim, K., and Zhou, Z.J. (2010). Role of ACh-GABA cotransmission in detecting image motion and motion direction. Neuron *68*, 1159–1172.

Petreanu, L., Gutnisky, D.A., Huber, D., Xu, N.L., O'Connor, D.H., Tian, L., Looger, L., and Svoboda, K. (2012). Activity in motor-sensory projections reveals distributed coding in somatosensation. Nature *489*, 299–303.

Rice, M.E., and Cragg, S.J. (2004). Nicotine amplifies reward-related dopamine signals in striatum. Nat. Neurosci. *7*, 583–584.

Rice, M.E., and Cragg, S.J. (2008). Dopamine spillover after quantal release: rethinking dopamine transmission in the nigrostriatal pathway. Brain Res. Brain Res. Rev. *58*, 303–313.

Shen, W., Hamilton, S.E., Nathanson, N.M., and Surmeier, D.J. (2005). Cholinergic suppression of KCNQ channel currents enhances excitability of striatal medium spiny neurons. J. Neurosci. *25*, 7449–7458.

Shuen, J.A., Chen, M., Gloss, B., and Calakos, N. (2008). Drd1a-tdTomato BAC transgenic mice for simultaneous visualization of medium spiny neurons in the direct and indirect pathways of the basal ganglia. J. Neurosci. *28*, 2681–2685.

Stuber, G.D., Hnasko, T.S., Britt, J.P., Edwards, R.H., and Bonci, A. (2010). Dopaminergic terminals in the nucleus accumbens but not the dorsal striatum corelease glutamate. J. Neurosci. *30*, 8229–8233.

Sullivan, M.A., Chen, H., and Morikawa, H. (2008). Recurrent inhibitory network among striatal cholinergic interneurons. J. Neurosci. *28*, 8682–8690.

Tang, A.H., Karson, M.A., Nagode, D.A., McIntosh, J.M., Uebele, V.N., Renger, J.J., Klugmann, M., Milner, T.A., and Alger, B.E. (2011). Nerve terminal nicotinic acetylcholine receptors initiate quantal GABA release from perisomatic interneurons by activating axonal T-type (Cav3) Ca^{2+} channels and Ca^{2+} release from stores. J. Neurosci. *31*, 13546–13561.

Threlfell, S., Clements, M.A., Khodai, T., Pienaar, I.S., Exley, R., Wess, J., and Cragg, S.J. (2010). Striatal muscarinic receptors promote activity dependence of dopamine transmission via distinct receptor subtypes on cholinergic interneurons in ventral versus dorsal striatum. J. Neurosci. *30*, 3398–3408.

Threlfell, S., Lalic, T., Platt, N.J., Jennings, K.A., Deisseroth, K., and Cragg, S.J. (2012). Striatal dopamine release is triggered by synchronized activity in cholinergic interneurons. Neuron *75*, 58–64.

Tritsch, N.X., Ding, J.B., and Sabatini, B.L. (2012). Dopaminergic neurons inhibit striatal output through non-canonical release of GABA. Nature *490*, 262–266.

Wilson, C.J., Chang, H.T., and Kitai, S.T. (1990). Firing patterns and synaptic potentials of identified giant aspiny interneurons in the rat neostriatum. J. Neurosci. *10*, 508–519.

Witten, I.B., Lin, S.C., Brodsky, M., Prakash, R., Diester, I., Anikeeva, P., Gradinaru, V., Ramakrishnan, C., and Deisseroth, K. (2010). Cholinergic interneurons control local circuit activity and cocaine conditioning. Science *330*, 1677–1681.

Yang, C.F., Chiang, M.C., Gray, D.C., Prabhakaran, M., Alvarado, M., Juntti, S.A., Unger, E.K., Wells, J.A., and Shah, N.M. (2013). Sexually dimorphic neurons in the ventromedial hypothalamus govern mating in both sexes and aggression in males. Cell *153*, 896–909.

Zhang, H., and Sulzer, D. (2004). Frequency-dependent modulation of dopamine release by nicotine. Nat. Neurosci. *7*, 581–582.

Zhao, S., Ting, J.T., Atallah, H.E., Qiu, L., Tan, J., Gloss, B., Augustine, G.J., Deisseroth, K., Luo, M., Graybiel, A.M., and Feng, G. (2011). Cell type–specific channelrhodopsin-2 transgenic mice for optogenetic dissection of neural circuitry function. Nat. Methods *8*, 745–752.

Zhou, F.M., Liang, Y., and Dani, J.A. (2001). Endogenous nicotinic cholinergic activity regulates dopamine release in the striatum. Nat. Neurosci. *4*, 1224–1229.

Neuron, Volume *81*

Supplemental Information

Striatal Cholinergic Interneurons Drive GABA Release from Dopamine Terminals

Alexandra B. Nelson, Nora Hammack, Cindy F. Yang, Nirao M. Shah, Rebecca P. Seal, and Anatol C. Kreitzer

Supplementary Figures

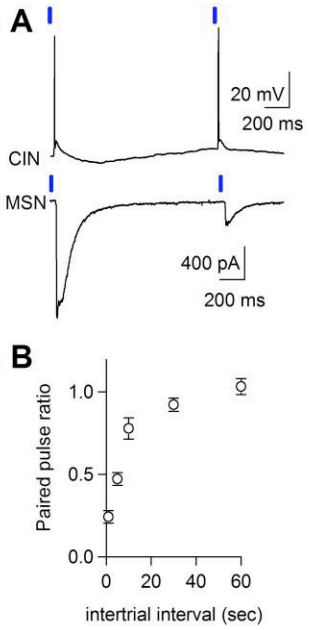

Figure S1. IPSCs triggered by activation of cholinergic interneurons show marked paired-pulse depression (Related to Figure 1).

A. Representative recordings from a ChR2-mCherry positive cholinergic interneuron (CIN) in current-clamp (upper panel) and a medium spiny neuron (MSN) in voltage-clamp (lower panel) during delivery of two light pulses (blue bars) at a 1 second intertrial interval. Action potentials were triggered in the cholinergic interneuron after each light pulse, but the IPSC following the second light pulse was attenuated. B. Summary of IPSC paired pulse ratio (PPR) with 1, 5, 10, 30, and 60 second intertrial intervals (n=5 MSNs). Error bars indicate SEM.

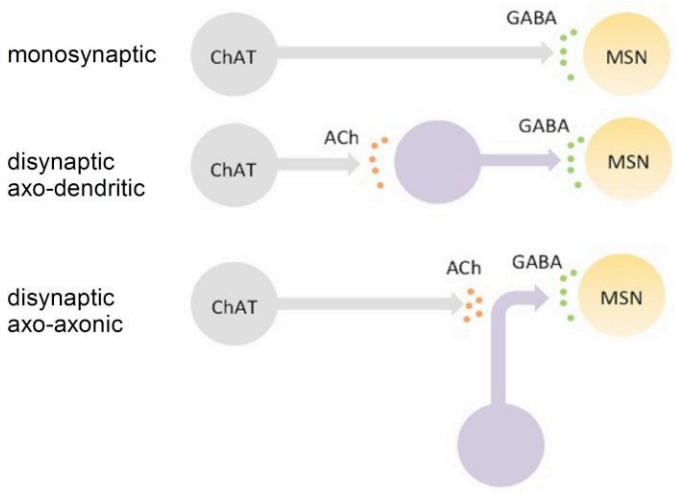

Figure S2. Schematic representation of different forms of synaptic inhibition (Related to Figure 2). Monosynaptic, disynaptic axo-dendritic, and disynaptic axo-axonic modes of synaptic transmission.

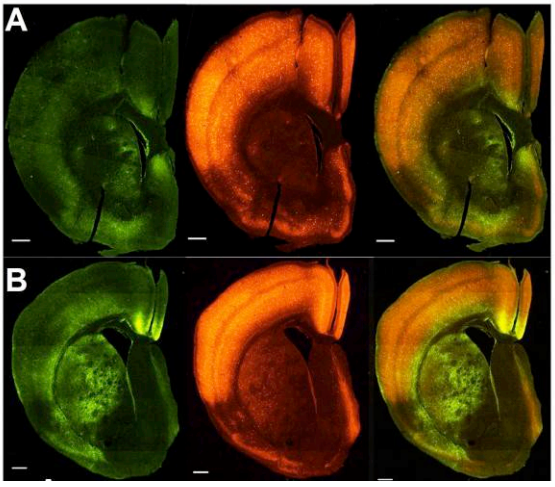

Figure S3. Co-infection with ChR2 and Caspase viruses in PV-Cre mice results in ablation of PV-positive striatal interneurons (Related to Figure 3).
Representative coronal sections containing the striatum (fixed and immunostained for parvalbumin (red) after patch-clamp recordings) from a parvalbumin (PV)-Cre mouse injected bilaterally with AAV1-DIO-ChR2-YFP (green) and unilaterally with AAV1-

FLEX-taCasp3-TEVp. A. Sections ipsilateral to caspase treatment. Left panel: ChR2-YFP, showing ablation of the majority of ChR2-YFP positive neurons in the dorsal striatum. Middle panel: parvalbumin positive cells in the same section are scanty and located around the edges of the striatum. Right panel: merged image demonstrating that these few remaining ChR2-YFP positive cells are also PV positive B. Sections contralateral to caspase treatment. Left panel: ChR2-YFP, showing robust ChR2-YFP expression in many neurons scattered throughout the dorsal striatum. Middle panel: parvalbumin positive cells in the same section are also scattered throughout the dorsal striatum. Right panel: merged image demonstrates ChR2-YFP was expressed in a large subset of PV-positive neurons.

Supplemental Experimental Procedures

Surgery

Surgeries were performed at 4-8 weeks of age. Anesthesia was induced with intraperitoneal ketamine/xylazine and maintained with inhaled isoflurane (1%). ChAT-Cre mice were stereotactically injected with AAV5-DIO-ChR2-mCherry (UNC vector core, 2 μL) in the bilateral dorsal striatum (+0.8 anterior, +/-1.5 lateral, and -2.5 mm inferior from bregma) through a small hole in the skull. PV-Cre mice were injected bilaterally with AAV5-DIO-ChR2-YFP (UNC vector core, 1 μL) and with AAV1-FLEX-taCasp3-TEVp (Yang et al., 2013), 2 μL in the left dorsolateral striatum (+0.8 anterior, -2.2 lateral, and 2.5 mm inferior). PV-Cre:ChAT-ChR2 mice were also injected with AAV1-FLEX-taCasp3-TEVp (2 μL) in the left dorsolateral striatum. Virus was injected at 0.2 μL/min, and the injection cannula was left in place for five minutes following each injection. After scalp closure and recovery from anesthesia, mice were given buprenorphine (50 ug/kg, intraperitoneal injection) and ketoprofen (5 mg/kg, subcutaneous injection) for postsurgical analgesia. Animals were returned to their home cages for 2-4 weeks prior to histological analysis or slice recordings.

A subset of ChAT-Cre mice were later re-anesthetized and the toxin 6-hydroxydopamine (1 μL, 5 mg/mL in normal saline) or normal saline (1 μL) was injected unilaterally into the medial forebrain bundle (-0.65 anterior, 1.2 lateral, -5 mm inferior). Desipramine (25 mg/kg, intraperitoneal injection) was given just prior to surgery in order to minimize neurotoxicity to other monoaminergic projections to the striatum. Following recovery from surgery, mice were returned to their home cages for 3-7 days prior to slice recordings.

Histology

A subset of mice were deeply anesthetized with intraperitoneal ketamine-xylazine and transcardially perfused with phosphate-buffered saline (PBS), followed by 4% paraformaldehyde in PBS. Brains were post-fixed overnight in the same fixative, then placed in 30% sucrose at 4° C for 2-3 days for cryoprotection. Brains were then frozen and cut into 30 μm coronal sections using a sliding microtome equipped with a freezing stage. Another set of sections were fixed overnight in 4% paraformaldehyde in PBS

following electrophysiological recordings, then placed in 30% sucrose at 4° C for 2-3 days, for subsequent histological analysis. These slices were then resectioned into 30 μm sections prior to staining.

Prior to staining, all slices were blocked in 10% normal donkey serum (NDS), 1% Triton-X in PBS for one hour. All washes were 0.5% Triton-X in PBS. Primary antibody (Millipore AB144P Anti-ChAT 1:500, SWANT Anti-parvalbumin 1:1000 or Pel-Freez P40101 Anti-Tyrosine Hydroxylase 1:1000) was added in 5% NDS, 1% Triton in PBS and incubated overnight at 4° C. After washing, slices were incubated with Alexa-Fluor 649-conjugated donkey anti-goat or donkey anti-rabbit secondary antibody (Invitrogen) for two hours at room temperature (RT). After additional washes, slices were mounted with Cytoseal 60 (ThermoScientific) and dried prior to imaging.

Counting of parvalbumin-positive neurons from slices used for physiological recordings was performed post-hoc in resectioned and PV immunostained slices ipsilateral and contralateral to the injection of AAV1-FLEX-taCasp3-TEVp. Only those cell bodies located in the dorsal half of the striatum in each coronal section were counted.

Physiology

Mice were deeply anesthetized with inhaled isoflurane, decapitated, and the brain was removed in ice-cold sucrose solution containing (in mM): 79 NaCl, 23 $NaHCO_3$, 68 sucrose, 12 glucose, 2.3 KCl, 1.1 NaH_2PO_4, 6 $MgCl_2$, and 0.5 $CaCl_2$. The brain was mounted on a submerged chuck, and sequential 300 μm coronal slices were cut on a vibratome (Leica), transferred to a chamber of warm (33° C) carbogenated ACSF containing (in mM) 125 NaCl, 26 $NaHCO_3$, 2.5 KCl, 1 $MgCl_2$, 2 $CaCl_2$, 1.25 NaH_2PO_4, 12.5 glucose for 30 minutes, and stored in carbogenated ACSF at room temperature. Each slice was then submerged in a chamber superfused with carbogenated ACSF at 31-33° C for recordings.

For recordings in ChAT-Cre mice, the zone of maximal ChR2-mCherry expression was identified under epifluorescence. Cholinergic interneurons were identified by mCherry fluorescence and large somata under differential interference contrast (DIC) optics. In ChAT-ChR2 mice, cholinergic interneurons were identified by their YFP-positive cell bodies. Medium spiny neurons were targeted for recordings by their non-

fluorescent cell bodies. In a subset of recordings from ChAT-Cre:Drd1a-tdTomato mice, direct pathway neurons were identified by their tdTomato-positive somata, and indirect pathway neurons were identified by their tdTomato-negative somata. Neurons were patched in whole-cell current-clamp or voltage-clamp configurations using glass electrodes (3-5 MΩ) filled with potassium-based physiologic (current-clamp) or cesium-based high-chloride (voltage-clamp) internal solution containing (in mM) respectively: 130 $KMeSO_3$, 10 NaCl, 2 $MgCl_2$, 0.16 $CaCl_2$, 0.5 EGTA, 10 HEPES, 2 Mg-ATP, 0.3 Na-GTP or 120 CsCl, 15 $CsMeSO_3$, 8 NaCl, 0.5 EGTA, 10 HEPES, 2 Mg-ATP, 0.3 Na-GTP, 5 QX-314, pH 7.3.

ChR2 was activated with 5 msec field illuminations through the 40X microscope objective. The light source was a mercury arc lamp (100W) gated with a TTL-controlled shutter (Uniblitz). The filter cube contained a D470/40x excitation filter and a cold mirror. Illumination intensity was adjusted to 1-3 mW, measured at the brain slice and calibrated using the aperture stop. In a subset of experiments to determine the paired-pulse ratio, two light pulses were delivered in succession with an interval between pulses between 0.1 and 60 seconds.

Light-evoked and carbachol-triggered IPSCs were recorded in the presence of NBQX (5 μM) and D-APV (50 μM) to reduce the contribution of glutamate release by cholinergic interneurons (Higley et al., 2011) and help isolate inhibitory synaptic responses.

Drugs

Drugs were prepared as concentrated stock solutions and diluted in ACSF for each experiment. NBQX (Tocris), Sulpiride (Tocris) and tetrabenazine (Sigma) were prepared in DMSO (Sigma), while D-APV (Tocris), dihydrobetaerythroidine (Tocris), scopolamine (Sigma), mecamylamine (Tocris), methyllycaconitine (Sigma), SCH23390 (Tocris) and picrotoxin (Sigma) were dissolved in water. IPSC amplitudes were measured following bath-application of drugs for a minimum of 10 minutes. Carbamoyl choline (Sigma) was dissolved in water and pressure ejected from a small glass pipette using a Picospritzer. Reserpine (Tocris) was dissolved in 1% glacial acetic acid, then diluted in water and administered at 5 mg/kg (intraperitoneal injection) 24 hours prior to

preparation of brain slices, and afterwards slices were treated continuously with ACSF containing 1 μM reserpine. Tetrabenazine was applied directly to brain slices (50 μM). Ro 4-1284 (Sigma) was dissolved in DMSO, diluted in saline, and administered at 15 mg/kg (intraperitoneal injection) one hour prior to slice preparation, and slices were then treated continuously in ACSF containing 10 μM Ro 4-1284, or placed in ACSF for at least one hour prior to recordings for the Ro 4-1284 washout condition.

Supplemental References

Higley, M.J., Gittis, A.H., Oldenburg, I.A., Balthasar, N., Seal, R.P., Edwards, R.H., Lowell, B.B., Kreitzer, A.C., and Sabatini, B.L. (2011). Cholinergic interneurons mediate fast VGluT3-dependent glutamatergic transmission in the striatum. PloS one *6*, e19155.

Yang, C.F., Chiang, M.C., Gray, D.C., Prabhakaran, M., Alvarado, M., Juntti, S.A., Unger, E.K., Wells, J.A., and Shah, N.M. (2013). Sexually dimorphic neurons in the ventromedial hypothalamus govern mating in both sexes and aggression in males. Cell *153*, 896-909.

Zhao, S., Ting, J.T., Atallah, H.E., Qiu, L., Tan, J., Gloss, B., Augustine, G.J., Deisseroth, K., Luo, M., Graybiel, A.M.*, et al.* (2011). Cell type-specific channelrhodopsin-2 transgenic mice for optogenetic dissection of neural circuitry function. Nature methods *8*, 745-752.